Scaling and localization of polaritonic states in piezoelectric Fibonacci superlattices

Zhenxing Liu and Weiyi Zhang
National Laboratory of Solid State Microstructures and Department of Physics, Nanjing University, Nanjing 210093, China
(Received 9 August 2005; published 24 October 2005)

The scaling and localization properties of polaritonic states in piezoelectric Fibonacci superlattices are studied using the generalized 4×4 transfer matrix method. The dynamics of electromagnetic waves and acoustic waves is treated on equal footing. Both polaritonic band structures and transmission spectra possess the pattern of the Cantorset with respect to generations. The scaling parameter $\alpha'=4.236$ is in agreement with the previous studies on pure electronic and phononic Fibonacci superlattices. Furthermore, the fractal nature of the transmission spectra serves as a proof for the (quasi)localization of polaritons which should be observable in experiments.

DOI: 10.1103/PhysRevB.72.134304 PACS number(s): 05.45.Df, 42.25.−p, 71.36.+c

Quasicrystal is a unique type of structure which lacks long-range translational symmetry but possesses a certain orientational order. The structural ordering of quasicrystals lies at the boundary between the translation invariant crystals and random glassy materials. Thus, the spectral properties of quasicrystals provide a way to understand how the extended states in crystals are transformed into the localized states in random glass when the translational symmetry is broken. For this reason, much research work has been carried out in the past 20 years, especially since the experimental discovery of the quasicrystal phase in an Al-Mn alloy with icosahedral symmetry.[1] Among them, the one-dimensional model systems described by the Fibonacci sequences have received the most attention since they contain the basic ingredients of quasicrystals and are relatively easy to deal with. Up to now, a variety of physical properties have been explored which involve superlattices with electronic,[2–7] vibrational,[8–11] dielectric,[12–17] as well as ferroelectric materials.[18–20] These studies suggest that the energy spectra of quasiperiodic systems have fractal structures and form Cantorsets. All states in the Fibonacci lattices are critically localized (quasilocalized).[21,22] For the current research status on quasiperiodic structures, one should consult the review article given by Albuquerque and Cottam where the characteristic spectral properties on superlattices with Fibonacci sequence, Thue-Morse sequence, and double-period sequence are analyzed and discussed in detail.[23]

In addition to the one-degree systems, both experimental and theoretical studies have been extended to other nonlinear as well as mode-coupled systems. In the nonlinear optical problems, the efficiency of high harmonics generation is greatly enhanced if quasiperiodic structures are adopted. The quasiphase matching is easily engineered using quasiperiodic structures since they offer more reciprocal lattice vectors than their periodic counterpart. Also the ultrasound spectra generated by the piezoelectric superlattices arranged in the Fibonacci sequences are studied; in particular, the possibility of creating the so-called polaritonic band gap in piezoelectric superlattices is proposed.[18,24] These studies take the long wavelength limit and apply only when the sample thickness is much shorter than the electromagnetic wavelength. The transmission spectra and scaling behavior of coupled phonon-photon states are not discussed. Since the quasiperiodic system is characterized by the scaling properties of its eigenmodes, and quasiperiodic piezoelectric superlattices are fundamentally different from those single-degree electronic, phononic, or photonic systems as it involves coupled photons and phonons, it is of great interest to analyze in detail the similarities and differences in their scaling behavior.

In this paper we consider the piezoelectric superlattices with Fibonacci sequences S_l as illustrated in Fig. 1. The superlattices can be prepared with an electric-field poling method.[25] The positively and negatively polarized domains with thickness $L_\pm$ are the two building blocks A and B. These building blocks are then arranged according to the concatenation rule $S_l=S_{l-2}S_{l-1}$ for $l\geqslant2$, with $S_0=B, S_1=A$. The number of layers is given by $NP=F_l$, where F_l is a Fibonacci number obtained from the recursive law $F_{l+1}=F_l+F_{l-1}$, with $F_0=1$ and $F_1=1$. We choose the two uniformly polarized domains above as our building blocks to facilitate a comparison either with the electronic systems in an incommensurate potential with two distinct on-site energies.[5,6] or with the dielectric superlattices with two distinct dielectric constants.[12,13,15,17] The scaling properties of eigenspectra of piezoelectric Fibonacci superlattices are obtained by comparing the polaritonic band structures and transmission spectra for consecutive generation l. Self-similarity structures are found with respect to generation. For particular frequencies and near its neighborhood, the spectra satisfy the scaling law for the lth and the $(l+3)$th generations. As the generation goes to infinite, the scaling parameter approaches $\alpha'=\tau^3=4.236$ with $\tau=(\sqrt{5}+1)/2$ denoting the golden mean. Transmission spectra show a self-similarity pattern with respect to either the generation or rescaled frequency. As indicated by the fractal feature in the transmission spectra, quasilocalization does exist in this system. However, because of the huge difference between the velocities of phonons and photons, superlattices larger than 20th generation (10 946 domains) are required in order to have a clear localization signature.

To maximize the coupling between photons and phonons in piezoelectric superlattices, one needs to have a setting that corresponds to the largest component of piezoelectric tensor. Figure 1 is such a setting for $LiNbO_3$; both the electric field $E_x(z,t)$ and lattice displacement $u_x(z,t)$ are in the x axis. The full dynamics of the system is described by the following coupled equation set:[26]

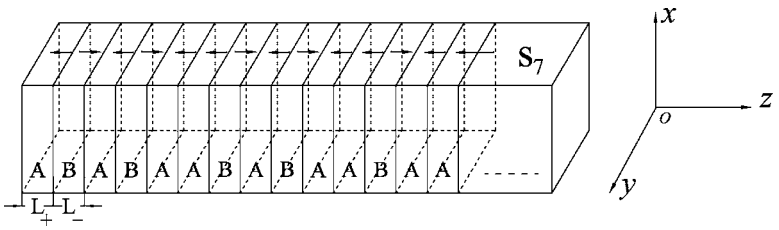

FIG. 1. The schematic diagram of a Fibonacci piezoelectric superlattice. Domains' polarization are along the $\pm z$ axis. The electric field and vibrational displacement are taken as the x axis.

$$\left(\frac{\omega L}{2\pi c_s}\right)^2 \bar{E}_x(\bar{z},\omega) = -\alpha\frac{\partial^2}{\partial\bar{z}^2}\bar{E}_x(\bar{z},\omega) - \beta\theta(\bar{z})\frac{\partial^2}{\partial\bar{z}^2}\left[\theta(\bar{z})\bar{E}_x(\bar{z},\omega)\right] + \beta\theta(\bar{z})\frac{\partial^3}{\partial\bar{z}^3}\bar{u}_x(\bar{z},\omega), \tag{1a}$$

$$\left(\frac{\omega L}{2\pi c_s}\right)^2 \bar{u}_x(\bar{z},\omega) = -\frac{\partial^2}{\partial\bar{z}^2}\bar{u}_x(\bar{z},\omega) + \frac{\partial}{\partial\bar{z}}\left[\theta(\bar{z})\bar{E}_x(\bar{z},\omega)\right]. \tag{1b}$$

The above equation set is written in a dimensionless form; the scaled variables and functions are defined as $\bar{z}=2\pi z/L$, $\bar{u}_x(\bar{z},\omega)=2\pi u_x(z,\omega)/L$, and $\bar{E}_x(\bar{z},\omega)=|d'_{15}(z)|E_x(z,\omega)$. $L=L_+ + L_-$ is the sum of thicknesses of two oppositely polarized domains. $\theta(\bar{z})=\pm 1$ identifies the left and right polarized domains. $c_s=1/\sqrt{\rho s'_{55}}$ is the tranverse sound velocity of the ferroelectric media. The two dimensionless material parameters are $\alpha=c^2/\bar{\epsilon}c_s^2$, $\beta=d'^2_{15}/\epsilon_0\bar{\epsilon}s'_{55}$. Later is the electromechanic coefficient which describes the coupling strength between photons and phonons. $\bar{\epsilon}=\epsilon-\Delta\epsilon$ is the effective dielectric constant and

$$\Delta\epsilon = \frac{1}{\epsilon_0}\left[\frac{d_{15}^2}{s'_{55}} + \frac{d_{16}^2}{s'_{66}} + d_{15}d_{16}\left(\frac{1}{s'_{56}} + \frac{1}{s'_{65}}\right)\right].$$

The reduced piezoelectric component is given by $d'_{15}(z)=d_{15}(z)+d_{16}(z)s'_{55}/s'_{65}$. The reduced elastic moduli are given by $1/s'_{55}=s_{66}/(s_{55}s_{66}-s_{56}s_{65})$, $1/s'_{66}=s_{55}/(s_{55}s_{66}-s_{56}s_{65})$, $1/s'_{56}=-s_{65}/(s_{55}s_{66}-s_{56}s_{65})$, and $1/s'_{65}=-s_{56}/(s_{55}s_{66}-s_{56}s_{65})$. For $LiNbO_3$,[27] $\alpha=1.6\times10^8$, $\beta=0.5923$. Note that the photon velocity is higher than the sound velocity by four orders of magnitude and their wavelengths set two different characteristic length scales in this system.

The above equations can be solved for homogeneous ferroelectric media. There are four eigensolutions for each domain. One pair represents renormalized electromagnetic modes, the other pair represents the renormalized acoustic modes, and the general solution can be expanded within these bases. After using the proper boundary conditions at domain interfaces, the electric field $\bar{E}_x$, vibrational amplitude $\bar{u}_x$, as well as their derivatives $\bar{E}'_x$ and $\bar{u}'_x$ at interfaces can be expressed in terms of transfer matrices for the left and right polarized domains,[26]

$$\begin{pmatrix} \bar{E}_x(\bar{L}_\pm,\bar{\omega}) \\ \bar{u}_x(\bar{L}_\pm,\bar{\omega}) \\ \bar{E}'_x(\bar{L}_\pm,\bar{\omega}) \\ \bar{u}'_x(\bar{L}_\pm,\bar{\omega}) \mp \bar{E}_x(\bar{L}_\pm,\bar{\omega}) \end{pmatrix} = M(\bar{L}_\pm,\bar{\omega}) \begin{pmatrix} \bar{E}_x(\bar{0},\bar{\omega}) \\ \bar{u}_x(\bar{0},\bar{\omega}) \\ \bar{E}'_x(\bar{0},\bar{\omega}) \\ \bar{u}'_x(\bar{0},\bar{\omega}) \mp \bar{E}_x(\bar{0},\bar{\omega}) \end{pmatrix}. \tag{2}$$

$\bar{\omega}=\omega L/2\pi c_s$ and the detailed expressions of transfer matrices are listed in Appendix A of Ref. 26. The transfer matrix of a given superlattice can be obtained by successive multiplications of $M(\bar{L}_\pm,\bar{\omega})$ with the prescribed sequence. Equation (2) forms the basis to study band structures and transmission spectra of this system.

The band structure for a given Fibonacci superlattice (S_l) is calculated, as customarily done, using the periodic boundary condition. This procedure ensures that the band structures approach the transmission spectra when generation l is large enough. The typical band structures are shown in Fig. 2 where the horizontal axis denotes the generation l while the

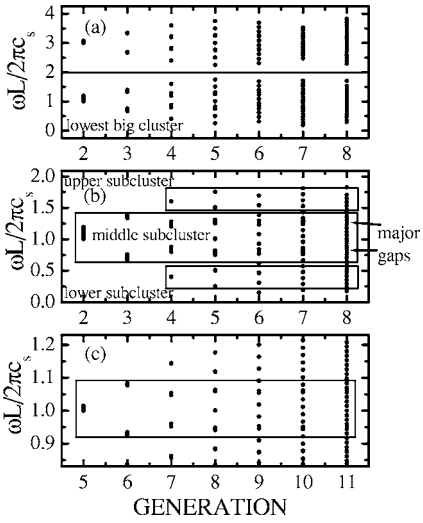

FIG. 2. Polaritonic forbidden gaps as a function of Fibonacci generation. The reduced domain sizes are $\bar{L}_+=\bar{L}_-=\pi$. (a) For generation $l=2\sim8$. (b) For generation $l=2\sim8$ but with the focus on a lower frequency. (c) For generation $l=5\sim11$, a frequency expanded view of (b) around $\bar{\omega}=1$. Notice the symmetrical patterns around the fixed points $\bar{\omega}=$odd integers.

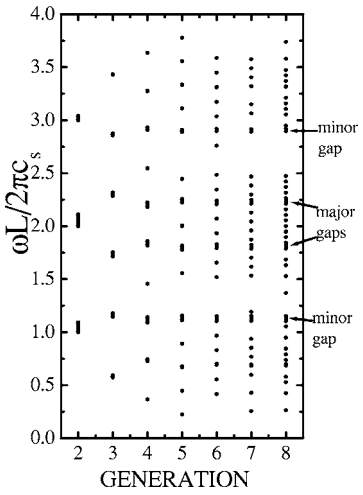

FIG. 3. Polaritonic forbidden gaps as a function of Fibonacci generation, the reduced domain sizes are $\bar{L}_+=1.5\pi$ and $\bar{L}_-=0.5\pi$. Notice the symmetrical pattern around the fixed point $\bar{\omega}=2$.

vertical axis denotes the forbidden gap resulting from the superlattice structure. In obtaining these figures, $\bar{L}_+$ and $\bar{L}_-$ are set as π. The forbidden gap indicates the range of forbidden modes for the coupled polaritons while uncoupled acoustic modes remain propagationlike. Figure 2(a) shows that there are infinite big clusters centered at the odd-integer frequencies $\bar{\omega}=1,3,5,\ldots$,. These frequencies actually correspond to the fixed points of the system under study and are determined by the acoustic wavelength in piezoelectric media. To unveil the self-similarity nature of the quasiperiodic system, the lowest big cluster centered around $\bar{\omega}=1$ is enlarged and replotted in Fig. 2(b) for an easy comparison with the spectra plotted in Fig. 2(c) differing by three generations. A clear physical picture that emerges from the spectra differing by three generations show a self-similar pattern. In fact, such properties are observed for any pair of spectra of generations l and $l+3$ and hold for other big clusters as well. Around the fixed points of frequencies, the difference between the lower edges of the forbidden gaps satisfies the scaling law, i.e., if the energy spectra are rescaled by a constant α', the lower edges of forbidden gaps of lth and $(l+3)$th generations will appear at almost the same locations.

Inspired by Ostlund *et al.*,[4] we have applied the renormalization operation on the matrix string. Simple analysis on the transfer matrices near the fixed points suggest that the traces of transfer matrices do recover after three cycles at fixed points, but the phases as argument in the trace are proportional to the total length of the superlattice. Thus, the scaling parameter α' is given by $\alpha'=\{\bar{L}_-F_{l+3}+(\bar{L}_+-\bar{L}_-)\mathrm{Int}[(F_{l+3}+1)/\tau]\}/\{\bar{L}_-F_l+(\bar{L}_+-\bar{L}_-)\mathrm{Int}[(F_l+1)/\tau]\}$ with $\tau=0.5(\sqrt{5}+1)$ denoting the golden mean. It approaches $\alpha'\to\tau^3=4.236$ when the Fibonacci generation goes to infinite. In addition, the three-cycle not only determines the band structures near the fixed points but also the band structure near each center of subclusters in the Cantor set. Note that the two major gaps around $\bar{\omega}=0.76$ and $\bar{\omega}=1.23$ in Fig. 2(b) seem to be insensitive to the Fibonacci generation, and they are also in good agreement with the transmission spectrum at large Fibonacci generation shown in Fig. 6.

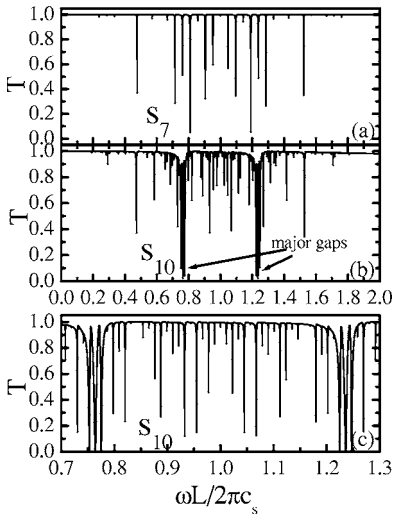

FIG. 4. The transmission spectra of finite Fibonacci superlattices with $\bar{L}_+=\bar{L}_-=\pi$. (a) Fibonacci sequence S_7 (21 layers); (b) S_{10} (89 layers); (c) a frequency expanded view of (b).

Although the scaling behavior is essentially determined by the Fibonacci sequences, the fixed points in both energy spectra and transmission spectra sensitively depend on the relative domain thicknesses. In Fig. 3 we show the energy spectra calculated with $\bar{L}_+=1.5\pi$ and $\bar{L}_-=0.5\pi$. The fixed points in this case are $\bar{\omega}=2,6,10,\ldots$, as can be checked by the trace mapping. The trace also recovers after three generations and spectra have the self-similar pattern. For the fixed point at $\bar{\omega}=2$, more subclusters and major gaps are observed due to the symmetry reduction of building blocks. In addition to the two major gaps around $\bar{\omega}=1.79$ and $\bar{\omega}=2.21$ which correspond to the ones in Fig. 2, two other minor gaps are observed around $\bar{\omega}=1.10$ and $\bar{\omega}=2.89$; all these gaps can be checked via the transmission spectra shown in Fig. 5.

While the electromagnetic wave and acoustic waves are coupled inside the piezoelectric superlattices, only the elec-

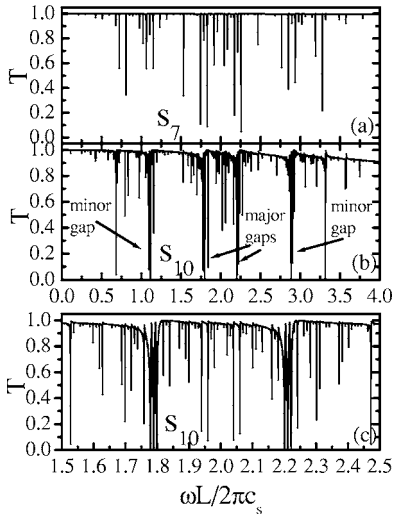

FIG. 5. The transmission spectra of finite Fibonacci superlattices with $\bar{L}_+=1.5\pi$ and $\bar{L}_-=0.5\pi$. (a) Fibonacci sequence S_7; (b) S_{10}; (c) a frequency expanded view of (b).

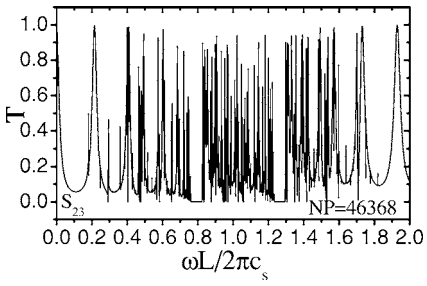

FIG. 6. The transmission spectrum of a Fibonacci superlattice S_{23} with $\bar{L}_+=\bar{L}_-=\pi$ (46 368 layers).

tromagnetic waves are coupled out for the configuration shown in Fig. 1 since the transverse elastic moduli of air is nearly zero. The representative transmission spectra for a set of Fibonacci sequences are shown in Fig. 4 with equal domain thickness $\bar{L}_+=\bar{L}_-=\pi$, Figs. 4(a) and 4(b) are the transmission spectra for Fibonacci sequences S_7 (21 layers) and S_{10} (89 layers), respectively. Figure 4(c) is a frequency enlarged view of Fig. 4(b) for easy comparison between the different generations. With respect to the fixed point of frequency at $\bar{\omega}=1$, a self-similarity pattern of the spectra is evident between S_7 and S_{10} sequences. The positions of the peaks correspond to each other well. Heights of the peaks are somewhat different due to the limited energy resolution adopted in the frequency mesh points. The transmission spectrum and the band structure are also in good agreement if one takes the different boundary condition into consideration. In fact, such scaling behavior in transmission spectra hold for every generation. We calculated up to S_{23}(46 368 layers), which indicates the quasilocalization of the eigenmodes.

For the asymmetrical domain structure studied in Fig. 3 with $\bar{L}_+=1.5\pi$ and $\bar{L}_-=0.5\pi$. The transmission spectra have similar scaling behavior around the fixed point of frequency at $\bar{\omega}=2$, the self-similarity pattern of the transmission spectra between S_7 and S_{10} are clearly shown in Fig. 5.

Unlike the forbidden band gaps shown in the band structures in Figs. 2 and 3, the band gaps as revealed in the transmission spectra are visible, but not clearcut. This is so because the sizes of the Fibonacci superlattices shown in Figs. 4 and 5 are much less than the wavelength of the electromagnetic wave and the wave nature of the electromagnetic fields has not emerged. In Fig. 6, a very large Fibonacci sequence S_{23} (46 368 layers) are considered with equal domain thickness. Clear band gaps have developed in the transmission spectrum which corresponds perfectly to the gaps observed in the band structure around $\bar{\omega}=0.76$–0.83 and $\bar{\omega}=1.23$–1.30, respectively. As we have mentioned before, the piezoelectric system is characterized by both the acoustic velocity and light velocity which differs by four orders of magnitude. The topological long-range order in space is on the order of the phonon wavelength and that is why the self-similarity features take place already at relatively low Fibonacci sequences while the electromagnetic wavelength is four orders of magnitude larger than the acoustic wavelength which amounts to several tens of thousands of layers.

To explore how the topological order affects the spectral properties, we have compared the transmission spectra of

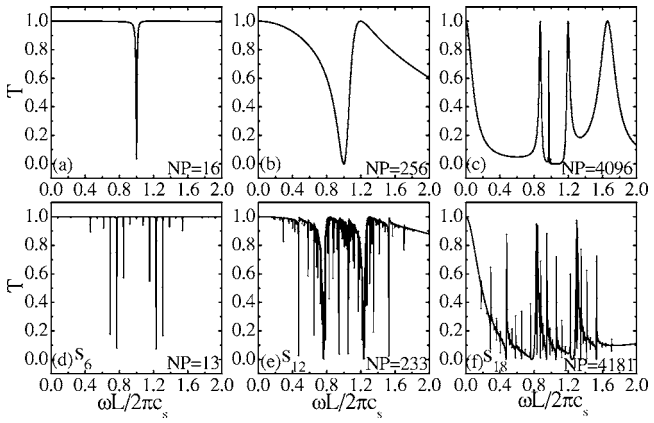

FIG. 7. The transmission spectra of periodic and Fibonacci superlattices with $\bar{L}_+=\bar{L}_-=\pi$. (a)–(c) Periodic superlattices with 16 (a), 256 (b), and 4096 (c) layers; (d)–(f) Fibonacci superlattices with 13 (d), 233 (e), and 4181 (f) layers.

superlattices for both periodic and Fibonacci sequences and they are illustrated in Fig. 7. Figures 7(a)–7(c) refer to the periodic superlattices with three different numbers of layers while Figs. 7(d)–7(f) refer to the Fibonacci superlattices with approximately the same number of layers. In the frequency range investigated and as the number of layers increases, only one polaritonic band gap develops for a periodic case at around $\bar{\omega}=1$ while there are two major polaritonic band gaps for the Fibonacci sequence at $\bar{\omega}=0.76$ and $\bar{\omega}=1.23$, respectively. As we said already, these gaps become well defined only when the sample size is comparable with the electromagnetic wavelength.

Using the global transfer matrix of a given Fibonacci sequence, the localization properties of eigenmodes can be analyzed by calculating directly the Lyapunov exponent $\Gamma(\bar{\omega})$;[28–30] the typical pattern of $\Gamma(\bar{\omega})$ is plotted in Fig. 8 for Fibonacci sequence S_{10}. One sees that there is a one-to-one correspondence between the transmission spectrum and the Lyapunov exponent. A high transmission means delocalized modes and vice versa. As the Fibonacci generation goes to infinite, all the eigenmodes become quasilocalized.

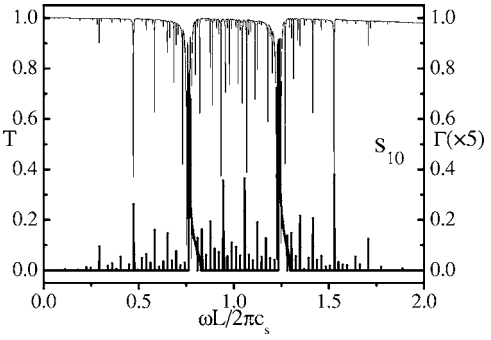

FIG. 8. The transmission spectrum (T, thinner curve) and the Lyapunov exponent (Γ, thicker curve) of the Fibonacci superlattice S_{10} with $\bar{L}_+=\bar{L}_-=\pi$.

In conclusion, we have studied in this paper the scaling and localization properties of polaritonic states in piezoelectric Fibonacci superlattices. The energy spectra of this photon-phonon coupled system possess the pattern of the Cantor set with respect to generations. The scaling parameter $\alpha' = 4.236$ obtained is in agreement with previous studies on pure electronic and phononic Fibonacci superlattices. Furthermore, the fractal nature of transmission spectra serves as proof for the (quasi)localization of polaritons which should be observable in experiments.

This work was supported in part by the State Key Program for Basic Research of China (Grant No. 2004CB619003). We wish to acknowledge the partial financial support from the NNSFC under Grants Nos. 10474040, 10334090, and "Excellent Youth Foundation" [10025419].

[1] D. Shechtman, I. Blech, D. Gratias, and J. W. Cahn, Phys. Rev. Lett. **53**, 1951 (1984).
[2] D. R. Grempel, S. Fishman, and R. E. Prange, Phys. Rev. Lett. **49**, 833 (1982).
[3] M. Kohmoto, L. P. Kadanoff, and C. Tang, Phys. Rev. Lett. **50**, 1870 (1983).
[4] S. Ostlund, R. Pandit, D. Rand, H. J. Schellnhuber, and E. D. Siggia, Phys. Rev. Lett. **50**, 1873 (1983).
[5] M. Kohmoto, Phys. Rev. Lett. **51**, 1198 (1983).
[6] M. Kohmoto, and Y. Oono, Phys. Lett. **102A**, 145 (1984).
[7] E. Diez, F. Domínguez-Adame, E. Maciá, and A. Sánchez, Phys. Rev. B **54**, 16792 (1996).
[8] R. Merlin, K. Bajema, R. Clarke, F.-Y. Juang, and P. K. Bhattacharya, Phys. Rev. Lett. **55**, 1768 (1985).
[9] S. Tamura, and J. P. Wolfe, Phys. Rev. B **36**, 3491 (1987).
[10] K. Mizoguchi, K. Matsutani, Shin-ichi Nakashima, T. Dekorsy, H. Kurz, and M. Nakayama, Phys. Rev. B **55**, 9336 (1997).
[11] D. H. A. L. Anselmo, A. L. Dantas, S. K. Medeiros, E. L. Albuquerque, and V. N. Freire, Physica A **349**, 259 (2005).
[12] M. Kohmoto, B. Sutherland, and K. Iguchi, Phys. Rev. Lett. **58**, 2436 (1987).
[13] W. Gellermann, M. Kohmoto, B. Sutherland, and P. C. Taylor, Phys. Rev. Lett. **72**, 633 (1994).
[14] T. Hattori, N. Tsurumachi, S. Kawato, and H. Nakatsuka, Phys. Rev. B **50**, R4220 (1994).
[15] E. Maciá, Appl. Phys. Lett. **73**, 3330 (1998).
[16] M. S. Vasconcelos and E. L. Albuquerque, Phys. Rev. B **59**, 11128 (1999).
[17] L. Dal Negro, C. J. Oton, Z. Gaburro, L. Pavesi, P. Johnson, A. Lagendijk, R. Righini, M. Colocci, and D. S. Wiersma, Phys. Rev. Lett. **90**, 055501 (2003).
[18] Y. Y. Zhu, N. B. Ming, and W. H. Jiang, Phys. Rev. B **40**, 8536 (1989); Y. Y. Zhu and N. B. Ming, *ibid.* **42**, 3676 (1990).
[19] Y. Q. Qin, H. Su, and S. H. Tang, Appl. Phys. Lett. **83**, 1071 (2003).
[20] G. Monsivais, J. A. Otero, and H. Calás, Phys. Rev. B **71**, 064101 (2005).
[21] M. Duneau and A. Katz, Phys. Rev. Lett. **54**, 2688 (1985).
[22] D. Levine and P. J. Steinhardt, Phys. Rev. B **34**, 596 (1986).
[23] E. L. Albuquerque and M. G. Cottam, Phys. Rep. **376**, 225 (2003).
[24] X. J. Zhang, Y. Q. Lu, Y. Y. Zhu, Y. F. Chen, and S. N. Zhu, Appl. Phys. Lett. **85**, 3531 (2004).
[25] M. Yamada, N. Nada, M. Saitoh, and K. Watanabe, Appl. Phys. Lett. **62**, 435 (1993).
[26] Weiyi Zhang, Zhenxing Liu, and Zhenlin Wang, Phys. Rev. B **71**, 195114 (2005).
[27] Y. Nakagawa, K. Yamanouchi, and K. Shibayama, J. Appl. Phys. **44**, 3969 (1973).
[28] Xiaoguang Wang, Uwe Grimm, and Michael Schreiber, Phys. Rev. B **62**, 14020 (2000).
[29] Enrique Maciá, Phys. Rev. B **60**, 10032 (1999).
[30] Enrique Maciá, Phys. Rev. B **61**, 6645 (2000).